Appl. Phys. B 73, 769–772 (2001)
DOI: 10.1007/s003400100744

Applied Physics B
Lasers and Optics

M. GREINER[1,2]
I. BLOCH[1,2,✉]
O. MANDEL[1,2]
T.W. HÄNSCH[1,2,*]
T. ESSLINGER[1,2]

Bose–Einstein condensates in 1D- and 2D optical lattices

[1] Ludwig-Maximilians-Universität, Schellingstr. 4/III, 80799 Munich, Germany
[2] Max-Planck-Institut für Quantenoptik, 85748 Garching, Germany

Received: 3 July 2001/Revised version: 26 September 2001
Published online: 23 November 2001 •

ABSTRACT Bose–Einstein condensates of rubidium atoms are transferred into one- and two-dimensional optical lattice potentials. The phase coherence of the condensate wavefunction in the lattice potential is studied by suddenly releasing the atoms from the trapping potential and observing the multiple matter-wave interference pattern of several thousand expanding quantum gases. We show how arbitrary phase gradients can be mapped onto the periodic wavefunction through the application of a potential gradient. Furthermore, the experimentally measured strength of the momentum components is compared to a theoretical model of the condensate wavefunction in the lattice.

PACS 03.75.Fi, 03.65.Nk, 05.30.Jp, 32.80.Pj

Bose–Einstein condensates in an optical lattice potential open up intriguing possibilities for the study of coherent matter in periodic potentials [1–7]. One remarkable feature of such a system is that almost all experimental parameters can be controlled with a high degree of precision. The lattice spacing, for example, can be controlled through the wavelength and the angle of the interfering laser beams, the lattice depth is adjustable over a wide range through the intensity of the interfering laser beams and in future experiments even the interaction strength between the atoms should be controllable via Feshbach resonances.

So far, the studies of Bose–Einstein condensates in periodic potentials have mainly been carried out in one-dimensional geometries. First experiments were directed towards the study of short optical standing wave pulses interacting with the condensate wavefunction [3, 4]. In further experiments condensates were adiabatically transferred into the new ground state of the periodic dipole force potential, to study tunneling processes, Josephson dynamics, superfluidity and Bloch oscillations [1, 5–7]. In deep standing wave potentials, number-squeezed states were investigated [2].

Here we show that magnetically trapped Bose–Einstein condensates can be efficiently transferred into two-dimensional lattice potentials by adiabatically increasing the lattice-potential depth. In the two-dimensional lattice potential the atoms are confined to an array of narrow potential tubes, where each tube is filled with a 1D quantum gas. The phase coherence of the condensate wavefunction throughout the lattice is studied by observing the multiple matter-wave interference pattern after a sudden release of the quantum gases from the trapping potential. Furthermore, we show that by pulsing-on linear potentials arbitrary phase gradients can be mapped onto the condensate wavefunction.

As in our previous work [8], Bose–Einstein condensates with up to 5×10^5 ^{87}Rb atoms are created in the $|F = 2, m_F = 2\rangle$ state with no discernible thermal component. The cigar-shaped condensates are confined in the harmonic trapping potential of a Quic-trap [9] with an axial trapping frequency of 24 Hz and radial trapping frequencies of 220 Hz. Such atom clouds have Thomas–Fermi radii of 45 μm along the axial and 4 μm along the radial directions (aspect ratio 11.3).

The lattice potential is formed by overlapping two perpendicular optical standing waves with the Bose–Einstein condensate as shown in Fig. 1. For this, the output of a near-infrared laser diode operating at a wavelength of $\lambda = 852$ nm is sent through a single-mode optical fiber and split into two perpendicularly propagating beams. These beams are focused onto the condensate with spot sizes w_0 ($1/e^2$ radius for the intensity) of approximately 75 μm. Both laser beams are then

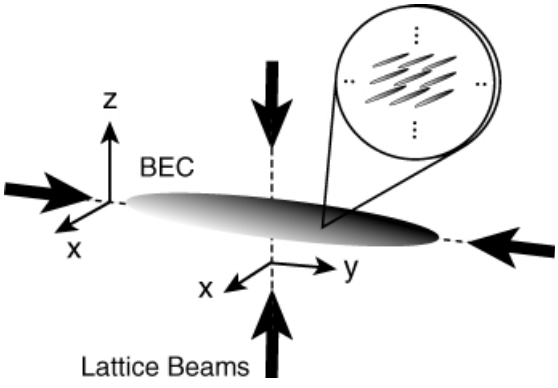

FIGURE 1 Schematic setup of the experiment. A 2D lattice potential is formed by overlapping two optical standing waves along the *horizontal axis* (y-axis) and the *vertical axis* (z-axis) with a Bose–Einstein condensate in a magnetic trap. The condensate is then confined to an array of several thousand narrow potential tubes (see *inset*)

✉ Fax: +49-89/285-192, E-mail: imb@mpq.mpg.de
*Also at: Department of Physics, University of Florence, Italy

recollimated with a lens pair and retroreflected to form a two-dimensional standing wave interference pattern at the position of the Bose–Einstein condensate. The far-off-resonant laser beam exerts an attractive force onto the atoms that is directed towards the intensity maxima of the light field [10]. The resulting potential for the atoms is directly proportional to the intensity distribution of the interfering laser beams and for the case of linearly polarized light fields it can be described by

$$U(y,z) = U_0 \left\{ \cos^2(ky) + \cos^2(kz) + 2\boldsymbol{e}_1 \cdot \boldsymbol{e}_2 \cos\phi \cos(ky)\cos(kz) \right\} . \quad (1)$$

U_0 denotes the potential maximum of a single standing wave, $k = 2\pi/\lambda$ is the magnitude of the wave vector of the lattice beams and $\boldsymbol{e}_{1,2}$ are the polarization vectors of the horizontal and vertical standing wave laser fields, respectively. The potential depth U_0 can be conveniently expressed in units of the recoil energy $E_\mathrm{r} = \hbar^2 k^2/2m$, where m is the mass of a single atom. The variable ϕ describes the time-phase difference between the two standing wave laser fields [11]. This time-phase difference is measured interferometrically and a piezo-mounted mirror in one of the standing wave optical pathways is used to actively stabilize the time-phase difference. In order to ensure a constant potential depth of the lattice potential throughout our measurement period, we have also stabilized the intensity of the lattice laser beams behind the optical fiber. The resulting two-dimensional interference pattern of the laser beams creates an array of narrow potential tubes, each filled with a quantum gas (see Fig. 1). These narrow potential tubes exhibit a highly anisotropic trapping geometry with large radial trapping frequencies ω_r of up to $2\pi \times 18\,\mathrm{kHz}$, for a potential depth of $U_0 = 12E_\mathrm{r}$ and weak axial trapping frequencies of $\omega_\mathrm{ax} = 2\pi \times 10$–$300\,\mathrm{Hz}$. The latter depend on the remaining confinement due the the magnetic trapping potential and due to the Gaussian beam profile of the lattice lasers.

The atoms are loaded into the combined trapping potential of the optical lattice and the magnetic trap by slowly increasing the intensity of the lattice beams to the final strength within 50 ms. Then the lattice light field and the magnetic trapping potential are suddenly turned off and the several thousand quantum gases expand and interfere with each other. A snapshot of the resulting interference pattern is obtained via absorption imaging after a variable time of ballistic expansion. An example of such an interference pattern can be seen in Fig. 2 for different time of flight values after the trapping potential has been switched off. Here the atoms were held in a two-dimensional optical lattice with a potential depth of $U_0 = 8E_\mathrm{r}$ and parallel polarization vectors ($\boldsymbol{e_1} \cdot \boldsymbol{e_2} = 1$). For orthogonal polarizations between the two standing wave laser fields or a time phase of $\phi = \pi/2$, the interference term in (1) vanishes and the potential is simply proportional to the sum of the intensities of the two standing wave light fields. In the corresponding momentum distribution (see Fig. 3, bottom row) the diagonal momentum components with $|p| = \sqrt{2}\hbar k$ are suppressed due to their vanishing geometrical structure factor. For parallel polarization vectors and a time phase of $\phi = 0$, interference between orthogonal laser beams leads to a significantly different lattice potential. In this configuration diagonal momentum components with $|p| = \sqrt{2}\hbar k$ (see Fig. 2) are present since now the associated geometrical structure factor does not vanish any more.

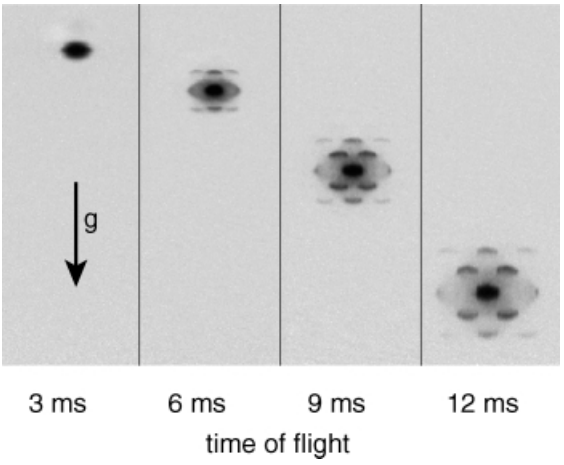

FIGURE 2 Absorption images of a Bose–Einstein condensate released from a two-dimensional periodic lattice potential with parallel polarization vectors $\boldsymbol{e}_1 \cdot \boldsymbol{e}_2 = 1$ and a potential depth of $U_0 = 8E_\mathrm{r}$ for different time of flight periods

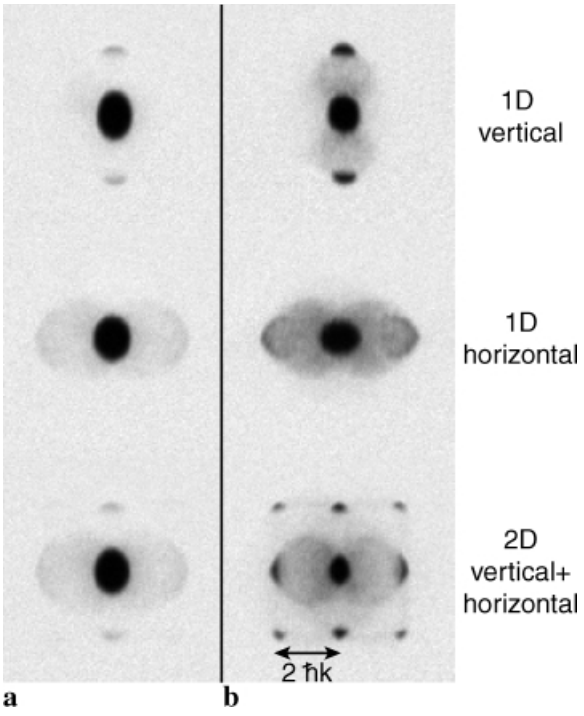

FIGURE 3 Absorption images of Bose–Einstein condensates released from one-dimensional vertical (*top row*), one-dimensional horizontal (*middle row*) and two-dimensional horizontal and vertical (*bottom row*) lattice configurations with orthogonal polarization vectors $\boldsymbol{e}_1 \cdot \boldsymbol{e}_2 = 0$. The images were taken for peak optical lattice depths of **a** $4E_\mathrm{r}$ and **b** $12E_\mathrm{r}$ after a time of flight of 15 ms

The influence of the lattice-potential depth on the interference pattern is shown in Fig. 3 for a one-dimensional vertical, a one-dimensional horizontal and a two-dimensional lattice potential. Several important features can be seen in these images. First, the higher-order momentum components become more intense as the potential depth is increased due to the tighter localization of the atomic wavefunctions on each lattice site. In addition, the horizontal momentum components

with $|p_y| = 2\hbar k$ appear curved. This is pronounced for the 1D horizontal standing wave configuration (see e.g. Fig. 3, middle row). When the different momentum components begin to separate in real space after the lattice potentials have been switched off, the repulsive mean-field potential acts like a defocusing lens for the higher-order momentum components. Due to the nonspherical distribution of the condensate wavefunction in the magnetic trap, this defocusing effect is much more pronounced along the horizontal direction, which has been confirmed in a 2D numerical simulation.

Second, s-wave scattering spheres become increasingly visible as the potential depth is increased. These spheres originate from collisions between the separating momentum components after the trapping potential has been switched off [12, 13]. The scattering probability is highest along the horizontal direction, which coincides with the long axis of the condensate and results in long interaction times.

We estimate the number of occupied lattice sites by counting the lattice sites within the Thomas–Fermi extension of the magnetically trapped condensate. Using the above condensate parameters we find that almost 3000 lattice sites are populated, with an average population of $\bar{N}_i$ of 170 atoms per site.

We have modeled the wavefunction $\Psi(\boldsymbol{r})$ of the Bose–Einstein condensate in the optical lattice as a sum of localized lattice wavefunctions $w(\boldsymbol{r}-\boldsymbol{r}_{k,j})$ on each lattice site (k, j) with a phase $\phi(\boldsymbol{r}_{k,j})$ weighted with a population factor $A(\boldsymbol{r}_{k,j})$:

$$\Psi(\boldsymbol{r}) = \sum_{k,j} A(y_k, z_j) w(x, y-y_k, z-z_j) \mathrm{e}^{\mathrm{i}\phi(y_k,z_j)} \,. \tag{2}$$

Here (y_k, z_j) denotes the two-dimensional position of the k, jth lattice site and $A(y_k, z_j)^2$ corresponds to the average number of atoms on the k, jth lattice site. The localized wavefunctions $w(\boldsymbol{r}-\boldsymbol{r}_{k,j})$ have been assumed to take the form of a Gaussian wavefunction in all three dimensions:

$$w(\boldsymbol{r}-\boldsymbol{r}_{k,j}) \propto \mathrm{e}^{-1/2\left\{((y-y_k)^2+(z-z_j)^2)/\sigma_\mathrm{r}^2 + x^2/\sigma_x^2\right\}}. \tag{3}$$

The effective widths of these wavefunctions are obtained by first calculating the ground-state extensions in the combined potential of the lattice and the magnetic trap, including effects due to the finite depth of the lattice potential. Then the additional broadening of the wavefunction due to the repulsive interactions between the atoms is considered by minimizing the ground-state energy of $\bar{N}_i$ atoms per lattice site through a variation of the widths of the Gaussian trial wavefunction (see [14]). For lattice depths of $U_0 = 12E_\mathrm{r}$ we find that the radial width of a single lattice wavefunction is on the order of $\sigma_\mathrm{r} = 0.12\lambda$. The maximum chemical potential per lattice tube μ_loc can then be calculated to be on the order of $\mu_\mathrm{loc} \approx h \times 5\,\mathrm{kHz}$, much smaller than the radial trapping frequencies of $\omega_\mathrm{r} \approx 2\pi \times 18\,\mathrm{kHz}$. Each quantum gas in a lattice tube is therefore in the 1D regime [15]. The resulting density distribution of the atoms in a central part of the lattice is displayed in Fig. 4a. A strong localization of the atoms on each lattice site can be seen for this potential depth. The corresponding momentum distribution can be directly obtained by Fourier transformation of the periodic wavefunction $\Psi(\boldsymbol{r})$. The experimentally measured number of atoms in a single higher-order momentum component with $p = 2\hbar k$ relative to the central $p = 0\hbar k$ component is compared with the theoretical prediction in Fig. 4b. The graph shows that the theoretical prediction is in good agreement with the experimental results.

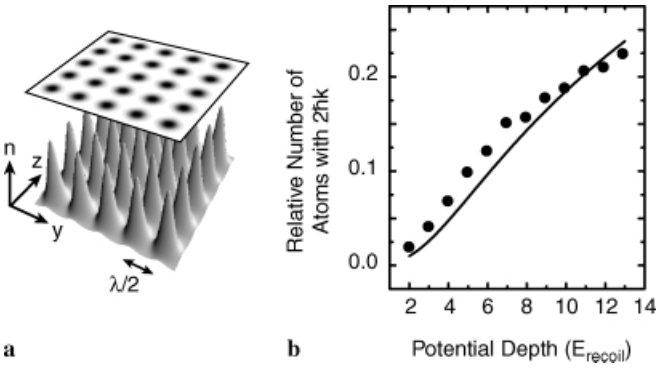

FIGURE 4 **a** Calculated density distribution of the atoms for a potential depth of $U_0 = 12E_\mathrm{r}$ assuming the theoretical model described in the text. **b** Fraction of atoms with momentum $p = +2\hbar k$ relative to the number of atoms with $p = 0\hbar k$ evaluated for the horizontal (y-)momentum component. The *solid line* is the theoretical prediction with no adjustable parameters

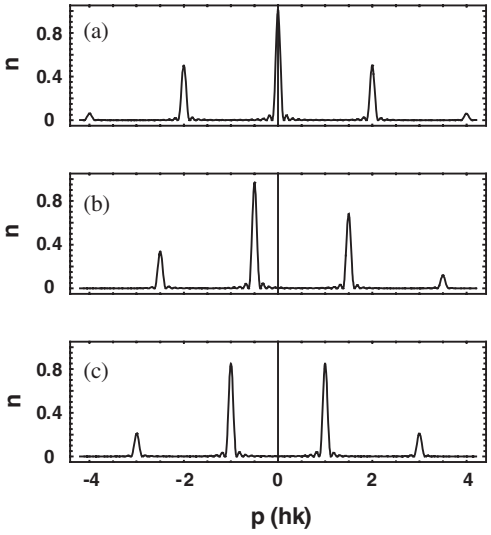

FIGURE 5 Theoretical momentum distribution for a one-dimensional periodic condensate wavefunction localized to $\sigma_\mathrm{r} = 1/15\lambda$ in each potential well. The phase differences between neighboring lattice sites are **a** $\Delta\phi = 0$, **b** $\Delta\phi = \pi/2$ and **c** $\Delta\phi = \pi$

Arbitrary phase gradients can be mapped onto the condensate in the periodic potential by exposing the atoms to a potential gradient. In a band-structure picture this is equivalent to being able to populate an arbitrary Bloch state within the first energy band. For simplicity we restrict the following discussion to a one-dimensional situation which can easily be extended to higher dimensions.

In order to prepare an arbitrary phase gradient we switch on an additional potential gradient V' which is directed along the lattice axis. Since each localized lattice wavefunction is now lifted to a different potential height, their phases also evolve differently with time [1]. The phase difference between neighboring lattice sites $\Delta\phi = \phi(x_{j+1}) - \phi(x_j)$ after a time t is then given by

$$\Delta\phi = -\frac{(V'\lambda/2)t}{\hbar} \,. \tag{4}$$

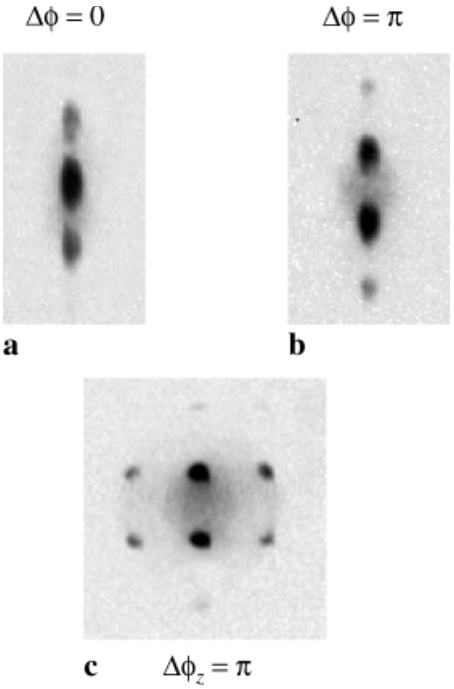

FIGURE 6 Experimentally measured momentum distributions after exposing the trapped periodic quantum gas to a potential gradient for a variable period of time. Momentum distributions of Bose–Einstein condensates that were stored in a one-dimensional standing wave potential: **a** with $\Delta\phi = 0$ and **b** with $\Delta\phi = \pi$ between neighboring lattice sites. **c** Momentum distribution of a Bose–Einstein condensate that was stored in a two-dimensional standing wave potential, with $\Delta\phi_z = \pi$. The time of flight in all images was 15 ms

As can be seen from (4) arbitrary phase differences between neighboring lattice sites can be achieved by turning off the potential gradient after a distinct time t, thereby creating a Bloch state with crystal momentum $q = V't/\hbar$. The resulting momentum distributions of the atoms can be seen in Fig. 5 for three phase differences $\Delta\phi = 0, \pi/2$ and π between neighboring lattice sites. In the experiment the phase gradients that have been mapped onto the condensate wavefunction are determined by evaluating the momentum distribution of the atoms after release from the trapping potential. This can be seen in Fig. 6a and b for the case of a one-dimensional vertical standing wave, for which the phase difference between neighboring lattice sites was set to $\Delta\phi = 0$ (Fig. 6a) and $\Delta\phi = \pi$ (Fig. 6b). The same idea can be applied to a Bose–Einstein condensate in a two-dimensional lattice potential as is shown in Fig. 6c. Here a magnetic field gradient of $B' = 20\,\mathrm{G/cm}$ was pulsed on for 450 µs along the vertical direction, resulting in a phase difference of $\Delta\phi_z = \pi$ between neighboring lattice sites. By applying a similar gradient along the horizontal direction, any Bloch state in the lowest-energy band of the two-dimensional lattice can be reached.

In conclusion, we have demonstrated that a Bose–Einstein condensate can be coherently transferred into the ground state of a one- and two-dimensional optical lattice potential. In the two-dimensional lattice the condensate consists of an array of narrow potential tubes, each filled with a 1D Bose–Einstein condensate. The coherence of the quantum gas in the lattice potential can be explored by monitoring the multiple matter-wave interference pattern after suddenly releasing the atoms from the trapping potential. Furthermore, we have shown that phase gradients can be mapped onto the periodic wavefunction by pulsing-on potential gradients for a suitable period of time. With the several thousand copies of 1D quantum gases in the two-dimensional optical lattice it seems possible to enter the regime of a Tonks gas [15–19], for which the crossover from bosonic to fermionic behavior of the atoms could be observed. By adding a third orthogonal standing wave, the atoms could in the future also be trapped in a three-dimensional light crystal with an average occupation number of up to 10 atoms per lattice site. In this setup it seems especially promising to reach the quantum-phase transition from a superfluid to a Mott-insulator phase [20] with an exact atom number in each lattice site.

REFERENCES

1 B.P. Anderson, M.A. Kasevich: Science **281**, 1686 (1998)
2 C. Orzel, A.K. Tuchman, M.L. Fenselau, M. Yasuda, M.A. Kasevich: Science **291**, 2386 (2001)
3 M. Kozuma, L. Deng, E.W. Hagley, J. Wen, R. Lutwak, K. Helmerson, S.L. Rolston, W.D. Phillips: Phys. Rev. Lett. **82**, 871 (1999)
4 J. Stenger, S. Inouye, A.P. Chikkatur, D.M. Stamper-Kurn, D.E. Pritchard, W. Ketterle: Phys. Rev. Lett. **82**, 4569 (1999)
5 S. Burger, F.S. Cataliotti, C. Fort, F. Minardi, M. Inguscio, M.L. Chiofalo, M.P. Tosi: Phys. Rev. Lett. **86**, 4447 (2001)
6 F.S. Cataliotti, S. Burger, C. Fort, P. Maddaloni, F. Minardi, A. Trombettoni, A. Smerzi, M. Inguscio: Science **293**, 843 (2001)
7 O. Morsch, J.H. Müller, M. Cristiani, D. Ciampini, E. Arimondo: Phys. Rev. Lett. **87**, 140402 (2001)
8 M. Greiner, I. Bloch, T.W. Hänsch, T. Esslinger: Phys. Rev. A **63**, 031401 (2001)
9 T. Esslinger, I. Bloch, T.W. Hänsch: Phys. Rev. A **58**, 2664 (1998)
10 R. Grimm, M. Weidemüller, Y.B. Ovchinnikov: Adv. At. Mol. Opt. Phys. **42**, 95 (2000) and references therein
11 A. Hemmerich, D. Schropp, T. Esslinger, T.W. Hänsch: Europhys. Lett. **18**, 391 (1992)
12 Y.B. Band, M. Trippenbach, J.P. Burke, Jr., P.S. Julienne: Phys. Rev. Lett. **84**, 5462 (2000)
13 A.P. Chikkatur, A. Görlitz, D.M. Stamper-Kurn, S. Inouye, S. Gupta, W. Ketterle: Phys. Rev. Lett. **85**, 483 (2000)
14 G. Baym, C.J. Pethick: Phys. Rev. Lett. **76**, 6 (1996)
15 D.S. Petrov, G.V. Shlyapnikov, J.T.M. Walraven: Phys. Rev. Lett. **85**, 3745 (2000)
16 M.D. Girardeau: J. Math. Phys. (NY) **1**, 516 (1960)
17 E.H. Lieb, W. Liniger: Phys. Rev. **130**, 1605 (1962); E.H. Lieb: Phys. Rev. **130**, 1616 (1963)
18 M. Olshanii: Phys. Rev. Lett. **81**, 938 (1998)
19 M.D. Girardeau, E.M. Wright, J.M. Triscari: Phys. Rev. A **63**, 033601 (2001)
20 D. Jaksch, C. Bruder, J.I. Cirac, C.W. Gardiner, P. Zoller: Phys. Rev. Lett. **81**, 3108 (1998)